



<https://doi.org/10.1038/s43247-022-00520-8>

OPEN

Future growth and decline of high mountain Asia's ice-dammed lakes and associated risk

Loris Compagno ^{1,2}, Matthias Huss ^{1,2,3}, Harry Zekollari ^{1,2,4}, Evan S. Miles ² & Daniel Farinotti ^{1,2}

Glaciers around the world are shrinking rapidly and will continue to do so in the next decades. Anticipating the consequences resulting from such glacier changes is key to design and implement adequate mitigation measures. Here, we focus on the future evolution of potential ice-dammed and supraglacial lakes in High Mountain Asia, as such lakes are responsible for the majority of glacier lake outburst floods in the region. We identify 11,129 potential lakes at present, with a total maximum volume of 2070 million m³. We find a strong correlation between large modelled lakes and historical outburst floods. By accounting for the evolution of glaciers under different climate change mitigation measures, we project that the number of potential ice-dammed lakes could increase by between 15 and 18% until 2080, with a concomitant 45–55% increase in their volume. Our findings thus suggest that a temporary increase of glacier lake outburst floods is to be expected in the coming decades.

¹Laboratory of Hydraulics, Hydrology and Glaciology (VAW), ETH Zurich, Zurich, Switzerland. ²Swiss Federal Institute for Forest, Snow and Landscape Research (WSL), Birmensdorf, Switzerland. ³Department of Geosciences, University of Fribourg, Fribourg, Switzerland. ⁴Laboratoire de Glaciologie, Université libre de Bruxelles, Brussels, Belgium. email: compagno@vaw.baug.ethz.ch

An increase in the number and size of glacier lakes has been observed during recent decades^{1–3}. These lakes not only enhance glacier mass loss^{4,5} but also present hotspots of hazard as they can retain large quantities of water^{6–9}. When glacier lakes drain, the downstream valleys can be affected by the resulting glacier lake outburst floods (GLOFs), which can lead to fatalities, damaged infrastructure, and ecological impacts^{10–12}. Between 1800 and 2021, moraine-dammed lakes caused an estimated total of 179 GLOFs in High Mountain Asia (HMA)¹³. Ice-dammed lakes (i.e., water blocked by ice at glacier margins) and supraglacial lakes (i.e., water blocked by ice on the glacier surface), instead, are believed to have caused 307 GLOFs¹³, i.e., 60% more events than moraine-dammed lakes.

This notwithstanding, most studies assessing potential hazards from GLOFs presently focus on single moraine-dammed and proglacial lakes^{9,14}, e.g., by modelling moraine-dam failure processes^{15,16} or by estimating the GLOF propagation pathway of related floods¹⁷. Other studies at regional scales focus on the past and future occurrence of GLOFs caused by moraine-dammed and proglacial lakes^{6,7,18}. These studies suggest that in the future, the size and number of moraine-dammed and proglacial lakes may increase, with a concomitant increase in GLOFs risk. Ice-dammed lakes, including supraglacial lakes, are generally neglected, albeit being inherently less stable and thus prone to GLOFs due to the brittle properties of the ice that dam them^{19,20}. In contrast to moraine-dammed lakes²¹, in fact, ice-dammed lakes can drain spontaneously via subglacial meltwater channels²² or due to mechanical failure of the ice dam²³. Predicting the location and the future evolution of potential ice-dammed lakes is thus essential to identify possible hazards. Indeed, early detection and observation can help in designing and implementing effective measures against GLOFs²⁴.

Here, we assess the location and temporal evolution of potential ice-dammed and supraglacial lakes (together referred to as "ice-dammed lakes" hereafter) for all glaciers in HMA, thus filling an important gap in available assessments. We consider all glaciers with a present-day area >2 km². First, we identify potential ice-dammed lakes in ice surface depressions and at the glacier margins for the year 2000. Then, we simulate the three-dimensional geometric evolution of each glacier by linking present-day digital elevation models (DEMs) to the output of GloGEMflow^{25,26}—a combined, regional-scale glacier mass balance, ice flow and supraglacial debris evolution model (see Methods). These simulations are performed under five shared socioeconomic pathways (SSP119, SSP126, SSP245, SSP370, and SSP585) from the sixth phase of the Coupled Model Inter-comparison Project²⁷. As the glaciers evolve over time, the evolution of future potential lakes is analysed, thereby capturing both the disappearance of individual lakes and the appearance of new ones. The simulations are performed by taking into account the enhanced melt caused by the lakes' presence^{4,28} (see Methods and Fig. 1).

A rigorous validation against lake extents mapped from satellite imagery (see Methods) and two recent studies targeting the recent evolution of HMA's glacier lakes^{2,29}, shows that the model (1) correctly detects the majority of existing lakes, (2) has skill in reproducing the evolution of glacier lakes during the past decades, and (3) provides reasonable estimates for the inferred lake depths and thus water volumes (see Fig. 2, Supplementary Results, and Figs. S1–S5).

Results and discussion

Temporal evolution of ice-dammed lakes. Our model projects that with strong (SSP119), medium (SSP245) and no (SSP585) climate change mitigation, 540⁷⁰¹₄₇₉, 569⁷⁵⁴₄₈₈ and 619⁸³⁰₅₁₀ glaciers,

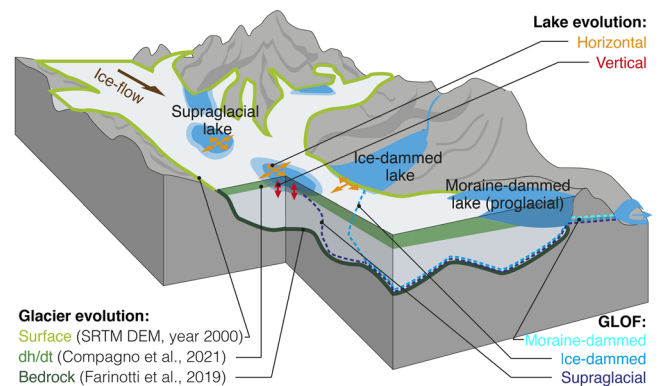


Fig. 1 Schematic overview of the different types of glacier lakes and the input data used in the present study. Data used for describing the glacier evolution are given in green. "dh/dt" stands for the ice thickness change rate. Glacier lakes are shown in blue, while red and orange arrows indicate their evolution. Dashed lines display possible lake drainage paths. Note that the study focuses on ice-dammed lakes (including supraglacial lakes). "GLOF" stands for Glacier Lake Outburst Flood.

respectively, will retain a total ice-dammed lake volume >1 million m³ at some stage during the period 2000–2100 (Fig. 3a; the superscript and subscript of the stated numbers define a 95% confidence interval, see Methods). Note that individual glaciers can have several lakes (see e.g., Figs. 2, 4, Figs. S6, and S7), and that the given threshold of 1 million m³ refers to the total lake volume per glacier.

For the year 2000, we detected 9327 potential ice-dammed lakes with a total area of 305 km² and a total volume of 1350 million m³ (Fig. 3d, e, f). By 2040, we project 11,731^{18,909}_{10,674} lakes with a total area of 344⁵⁴⁸₃₁₈ km² and a total volume of 2450³³⁰⁰_{2,100} million m³, mostly independent from the climate change mitigation measures. Between 2040 and 2080, the number, area and volume of potential ice-dammed lakes all tend to increase less for strong climate change mitigation measures (SSP119) than for scenarios with no climate change mitigation (SSP585). This is because stronger mitigation implies less warming, and thus slower expansion of future ice-dammed lakes due to different glacier geometry evolution, leading to the formation of fewer and smaller ice-dammed lakes.

By 2100 and for strong climate change mitigation measures (SSP119), the increase in area, volume, and number of ice-dammed lakes is expected to slow down, reaching 361⁶⁹⁴₂₈₉ km², 3110⁴⁶⁴⁰₂₃₈₀ million m³, and 12,292^{17,775}₉₄₈₂, respectively. With no climate change mitigation (SSP585), these numbers decrease due to glacier retreat to 290⁶³⁹₂₀₄ km², 2870⁴⁹²⁰₁₉₃₀ million m³, and 10,068^{13,538}₆₉₈₁, respectively. With medium to no climate change mitigation (SSP245 and SSP585), these quantities are projected to peak in the second half of the century, the maximum occurring earlier but being slightly lower for low-emission scenarios (Fig. 3d, e, f). For SSP245, for example, the maximal volume of potential ice-dammed lakes will be reached around 2095, whilst for SSP585 it will be reached around 2080 (Fig. 3d, e, f).

Regional differences. The location and evolution of the potential ice-dammed lakes shows pronounced regional differences (Fig. 5, Figs. S8, S9 and S10). Eighteen of the 50 largest potential ice-dammed lakes (stars in Fig. 5) are located in the Karakoram. This region also presents the highest total lake volume when spatially aggregated on a 1° × 1° grid (spheres in Fig. 5), and shows the latest peak in potential maximum lake volume. With the medium emission scenario SSP245, this maximum in lake volume is

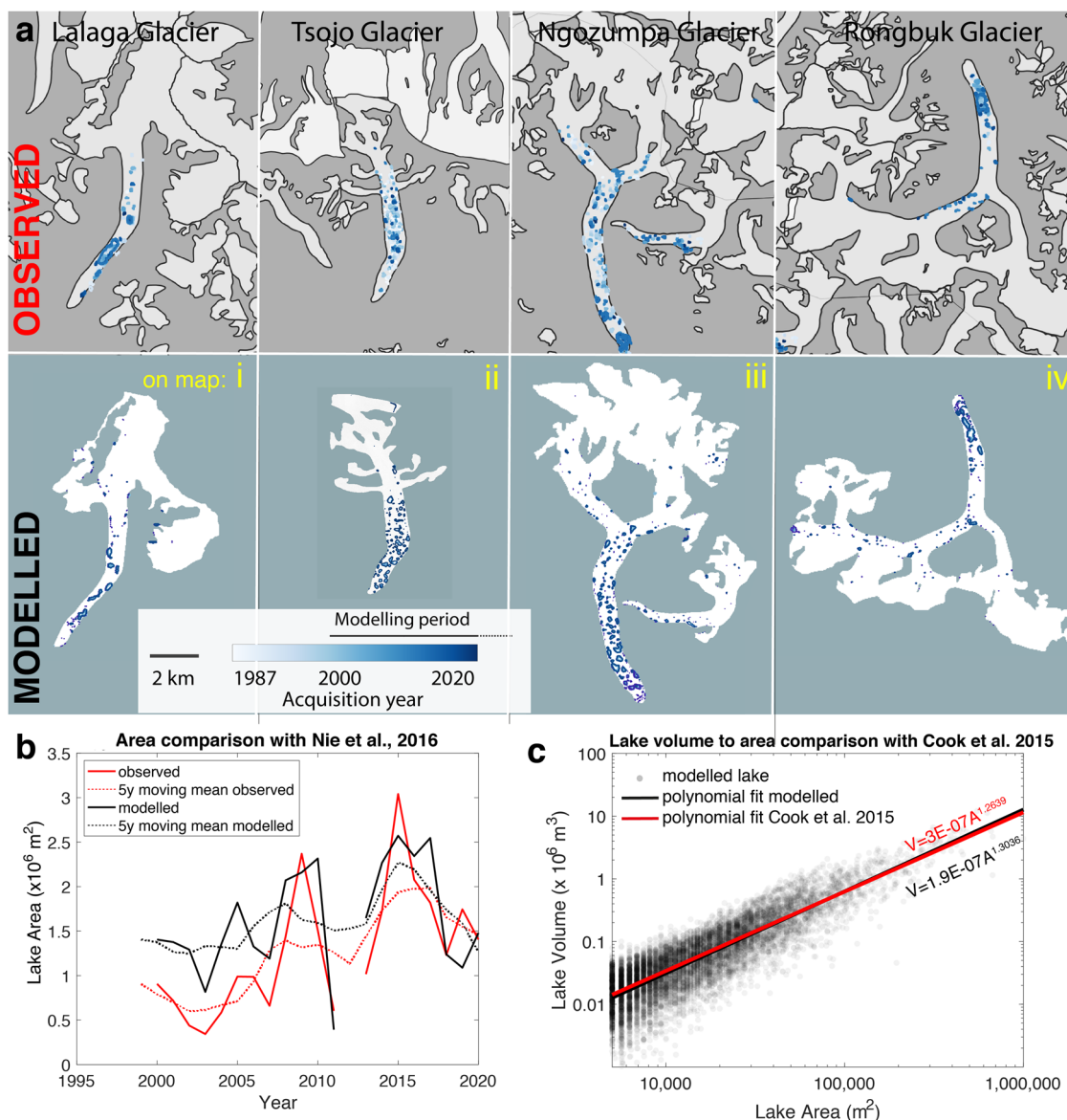


Fig. 2 Validation of model results. **a** Qualitative comparison between observed lakes between 1987 and 2020^{2,67} and model results (1999–2020) for Lalaga, Tsojo, Ngozumpa and Rongbuk glaciers. Glacier locations are shown by yellow roman numerals in Fig. 5. **b** Evolution of the total area for observed ice-dammed lakes^{2,67} and model results for the four glaciers in (a). Each observed lake is compared with the closest modelled lake, and the results are then aggregated per year. Note that there were no observations in 2012. **c** Relationship between lake area and lake volume as observed⁶⁵ (red) and modelled (black). Each black circle is a modelled lake, while the black line is a second-order polynomial fit. The polynomial fit of Cook et al. 2015 (ref. ⁶⁵) is based on nine observed supraglacial lakes.

projected to occur between 2070 and 2090 (Fig. 5 and Fig. S8). In the Himalayan range, the potential lake volume is instead anticipated to peak earlier, typically between 2040 and 2050 (see Fig. 5 and Fig. S9). This reflects the regional pattern in glacier mass changes: in the Karakoram, glaciers showed balanced mass budgets until recently^{30,31}, while glaciers in e.g., the Eastern Himalaya, Southern and Eastern Tibet, or the Hengduan Shan, experienced a negative mass balance^{32,33}. This regional diversity is linked to differences in climate evolution, glacier hypsometries, glacier size, and sensitivities to changes in climate^{30,31}. Since these factors will continue to influence the evolution of glaciers throughout the 21st century^{33–35}, they also exert control on the evolution of the future ice-dammed lakes.

Of note is the fact that the inferred spatial distribution corresponds to that of reported GLOFs¹³: GLOFs from ice-dammed and supraglacial lakes primarily occurred in the

Karakoram (Fig. 5), thus overlapping with the region where we model the majority of large ice-dammed lakes. GLOFs due to moraine failure have principally occurred in the Central and Eastern Himalayas, coinciding with the regions where glaciers thinned and retreated strongly in recent decades^{31,32,36,37} and where the modelled potential lake volume peaks the earliest (that is between 2040 and 2050).

Large potential ice-dammed lakes and link to observed GLOFs.

The large majority of historically observed GLOFs from ice-dammed and supraglacial lakes originated from a relatively small number of individual glaciers¹³, all of which developed large ice-dammed lakes in our modelling (Fig. 6). 38 of the 39 GLOFs (97%) that were observed from ice-dammed lakes since 2000, for example, stem from the 6% of glaciers with the largest modelled lake volumes. Similarly, all 14 GLOFs from supraglacial lakes that

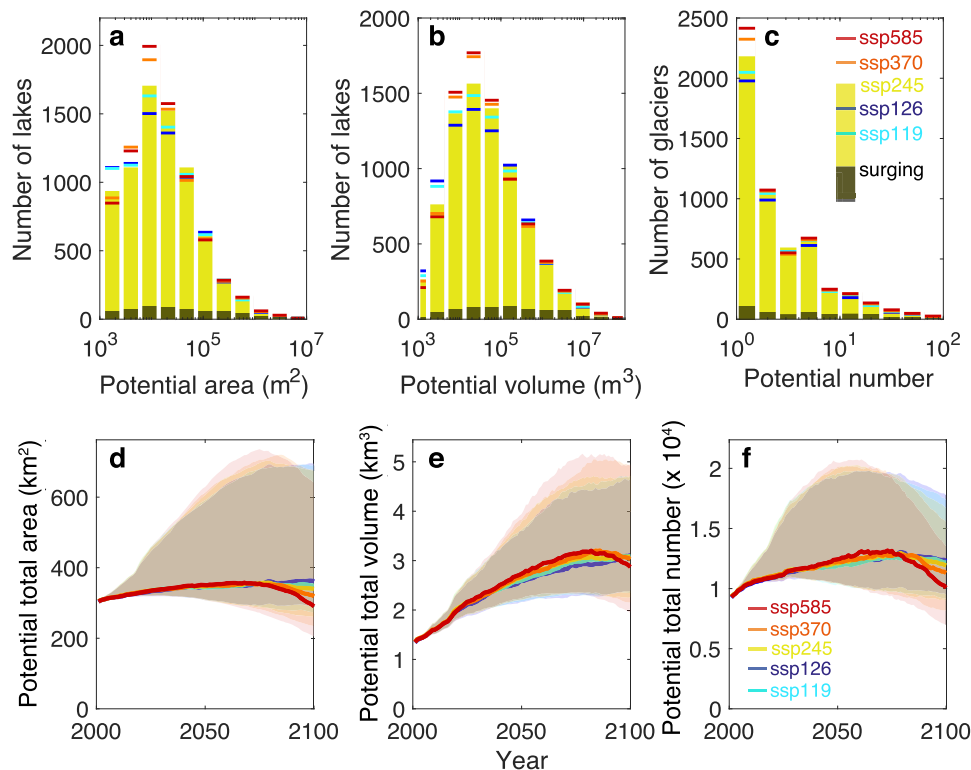


Fig. 3 Size distribution and temporal evolution of ice-dammed lakes across HMA throughout the 21st century. Distributions of the (a) area, (b) volume, and (c) number of ice-dammed lakes are given for the time of modelled maximum lake extent, volume, and number, respectively. Surge-type glaciers are recognised on the basis of the inventory of ref. ⁶⁸. Results are divided into SSP scenarios (coloured bars and lines), while surge-type glaciers are displayed by black bars. Evolution of the total (d) area, (e) volume, and (f) number of ice-dammed lakes. The shaded bands depict a 95% confidence interval derived from uncertainties in the different model parameters (see Methods).

were observed since 2000 stem from the 20% of glaciers with the largest modelled lake volumes. A strong relationship exists between modelled lake volume and observed historical GLOFs, thus indicating that the modelled volumes can be used as an indicator for actual hazard. In this sense, the high number of large ice-dammed lakes for which no GLOF is yet documented to date could provide hints for where GLOFs might occur in the future. The degree to which the modelled increase in ice-dammed lakes will translate into an actual increase in GLOFs remains to be seen, whilst it is clear that an increase in lake volumes would increase the magnitude of the potential GLOFs³⁸.

Inspection of our results at the scale of individual glaciers suggests that the model does well in identifying known, large glacier lakes that are prone to drainage. An example (see Supplementary Results for two additional ones) is the ice-dammed lake at the margin of Kyagar Glacier, Chinese Karakoram^{12,39}. According to our simulations, the Kyagar lake had the potential to contain up to 190 million m³ of water (when completely filled) around the year 2003 (Fig. 4), which is in good agreement with the 153 million m³ inferred in a dedicated study³⁹. This lake generated 44 GLOFs since 1880¹³, and repeatedly caused damages amounting to several tens of millions USD to the infrastructure downstream¹¹. Our modelling predicts that the maximal potential volume of this lake will diminish in future, until disappearing due to glacier retreat by the end of the century (Fig. 4). Although this suggests that the magnitude of GLOFs from Kyagar Glacier will decrease in the future too, we note that the glacier is of surge-type⁴⁰, i.e. subject to sudden advances without direct climatic control⁴¹. Such dynamics are not accounted for by our model, and a glacier re-advance during a surge could result in the formation of new, potentially large ice-dammed lakes. Surges are neglected in our model as they are not predictable from current

knowledge, despite important advances recently achieved in the field⁴².

We also note that the model identifies lakes that are missing from the inventories of e.g., ref. ^{2,29}, such as modelled lakes for two unnamed glaciers (labelled "RGI60-13.36942" and "RGI60-13.49295" in the Randolph Glacier Inventory version 6⁴³) and Monomaha Glacier (Fig. S6). The actual existence of these lakes was confirmed through attentive inspection of satellite imagery (e.g., Fig. S2), thus suggesting that (i) the model results could be helpful in supporting current monitoring efforts⁴⁴, and (ii) currently-available lake inventories might have difficulties in detecting lakes that are ice- and snow-covered during large parts of the year or lakes that are not permanent⁴⁴. When projecting the evolution of these previously unidentified glacier lakes into the future, contrasting patterns emerge. On the one hand, the lake of glacier RGI60-13.36942 is anticipated to increase in size due to enhanced melting. On the other hand, glacier retreat causes the lakes for both Monomaha Glacier and glacier RGI60-13.49295 to disappear after mid-century. We note that no GLOFs have been reported for these lakes¹³ despite of their size, and that whilst being an indication for enhanced risk, the presence of an ice-dammed lake does not imply that a destructive outburst flood will actually occur.

Finally, the model also projects the emergence of new, large ice-dammed lakes, which might become important targets for future monitoring. Examples are given by a further unnamed glacier (RGI60-13.24745), Belmonomaha Glacier, and Lalanga Glacier (Fig. S7). Indeed, our modelling suggests that the interplay between retreating ice and local bedrock topography could generate new depressions, some of which could develop into lakes exceeding 10 million m³ in volume. A list of the 50 largest modelled lakes is provided in Table S1. Considering the

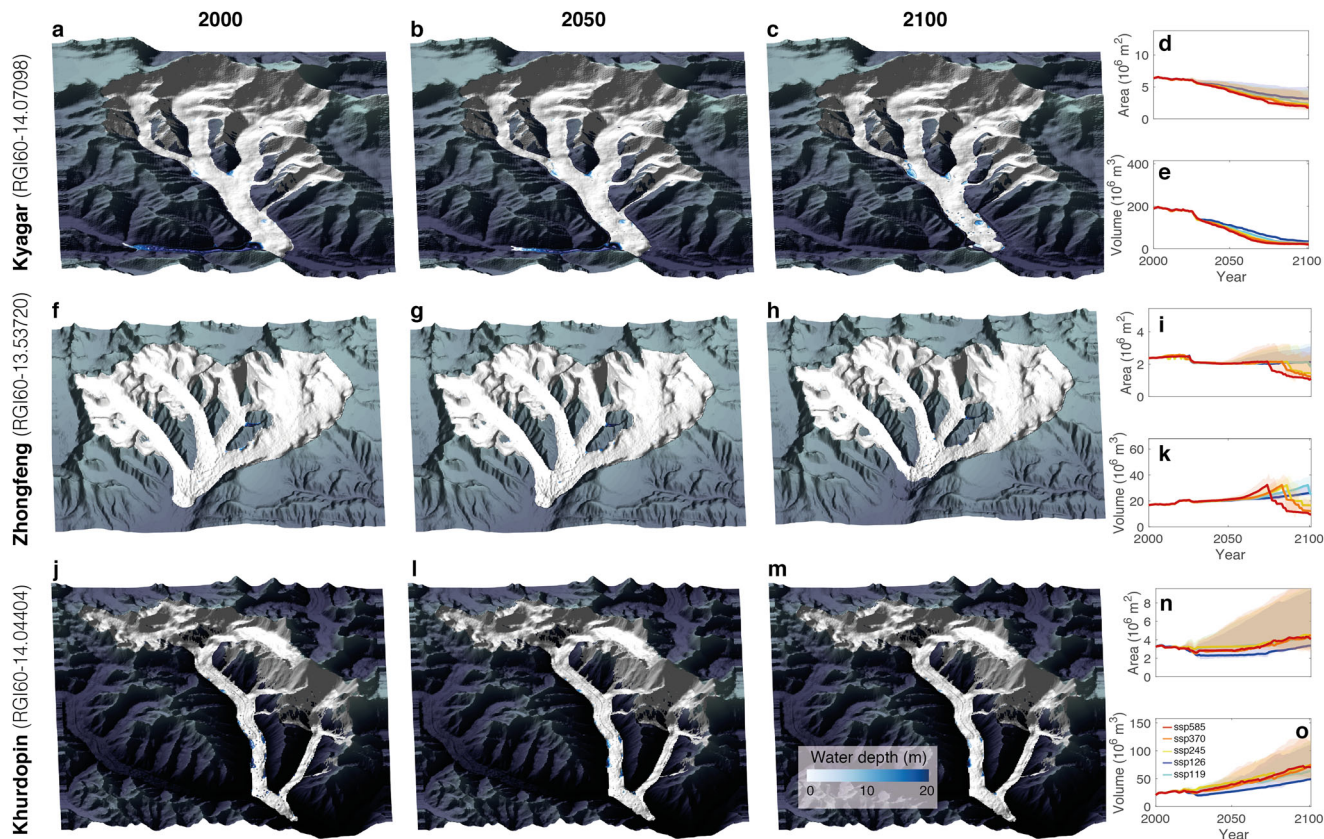


Fig. 4 Evolution of ice-dammed lakes for three selected glaciers. The modelled evolution of both the glacier geometry and the ice-dammed lakes is shown for (a-c) Kyagar, (f-h) Zhongfeng and (j, l, m) Khurdopin Glaciers. The columns refer to the years 2000, 2050 and 2100. The lake colour shows the lake depth with a scale given in (m). d, i, n Area and (e, k, o) volume evolution of all potential ice-dammed lakes for each glacier.

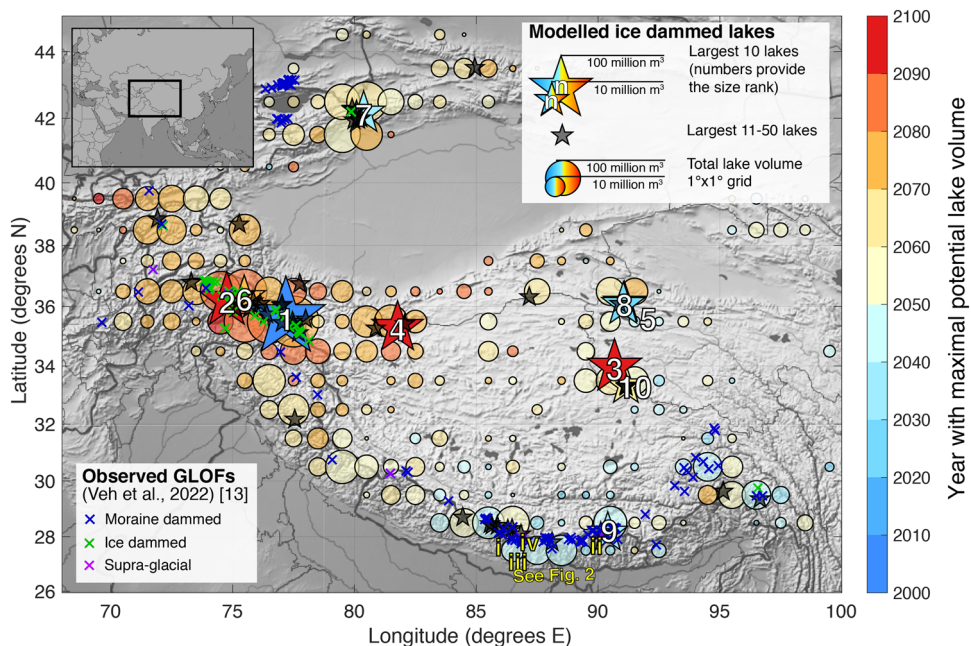


Fig. 5 Regional distribution of ice-dammed lakes and observed historical GLOFs in HMA. The map shows the ten largest modelled ice-dammed lakes by volume (coloured stars; rank given by white numbers; the star's size is proportional to the lake volume), the 11-50 largest modelled lakes (transparent stars without numbers), and the maximal lake volume aggregated for a 1° x 1° grid (coloured spheres, the size is proportional to the aggregated lake volume). The colour of both the stars and the spheres correspond to the decade in which the maximal lake volume is reached. Coloured crosses indicate observed GLOFs¹³ and distinguish between three categories (legend given at bottom left). The yellow roman numerals correspond to the locations of the four glaciers shown in Fig. 2. Background map source: Natural Earth.

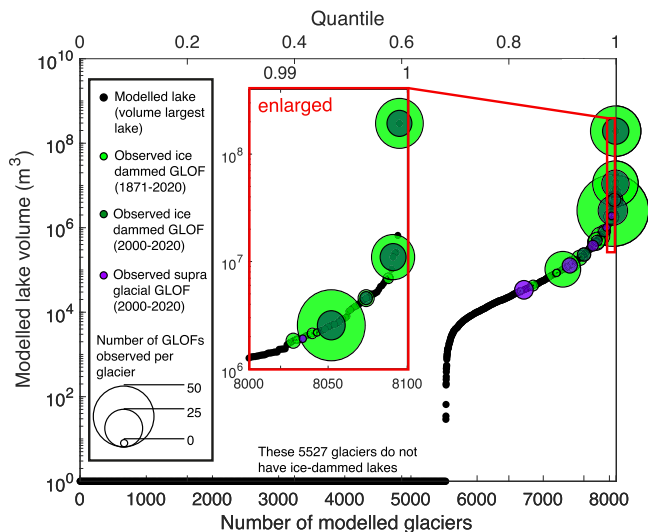


Fig. 6 Relation between observed GLOFs¹³ and modelled ice-dammed lakes. The black dots (appearing like a line when close together) show the modelled maximum lake volume for each glacier (under SSP245). Glaciers are sorted by total lake volume, with the first ca. 5600 glaciers not showing any ice-dammed lake formation at all. The green and purple spheres are observed GLOFs from ice-dammed and supraglacial lakes¹³, respectively. GLOFs from ice-dammed lakes before (light green) and after (dark green) 2000 are distinguished (2000 marks the start of our simulations, i.e., the acquisition year of the digital elevation model⁵⁰, see Methods), and the size of the spheres depicts the number of GLOFs observed per glacier. Note that most GLOFs overlap with large modelled lakes.

strong relation identified between modelled lake volumes and past GLOFs (cf. Fig. 6), we suggest that these sites deserve attention, and that their future evolution should be carefully monitored.

Limitations and implications for risk mitigation. Although our results can have implications for the planning of future risk mitigation measures, we caution against their over-interpretation: the model shows encouraging performance in both qualitative and quantitative comparisons with observations (see Fig. 2, Supplementary Results and Figs. S1–S5) but is also affected by a number of simplifications that are unavoidable when representing the evolution of glaciers and lakes at a regional scale. Most importantly, we emphasise the use of the word "potential" in our results for potential ice-dammed lakes. The wording is meant to stress that not every glacier depression should be expected to become water-filled. Indeed, assessing each depression's ability to actually retain water would require detailed information on the local ice dynamics, drainage patterns, topography, and climate. The geometrical evolution of ice-dammed lakes, moreover, is dependent on a number of factors including water temperature, stratification, inflow rate and location, or even water turbidity^{45–49}. Such data do not exist at the regional scale, which made us opt for a simple, parameterised approach. The data used as input to our model (e.g., the surface DEM) are subject to uncertainties too, or are themselves an output of a regional model (e.g., climate data, glacier ice thickness, or debris thickness). This introduces an additional layer of uncertainty that is difficult to quantify. Finally, it is difficult to constrain some of the involved processes at all. A number of ice-dammed lakes in HMA, for example, are known to form in combination with glacier-surge events, and as long as glacier surging remains unpredictable, so will be the development of related ice-dammed lakes. To quantify the most important uncertainties, we re-computed the evolution

of all ice-dammed lakes with altered model parameters in our lake-evolution scheme (see Methods). The resulting uncertainty is relatively large (Fig. 3d–f) but the general pattern for the temporal evolution appears to be robust: the number and volume of ice-dammed lakes will increase independently of the climate change mitigation measures, but will peak later for strong climate-mitigation scenarios as a result of slower glacier retreat.

Our results provide a first assessment of the future evolution of ice-dammed lakes at the scale of HMA. Ice-dammed lakes are responsible for the majority of observed GLOFs, yet these have been largely ignored by regional studies due to their dependence on local conditions. We addressed this gap by coupling a parameterisation of glacier lake evolution with a regional-scale glacier model. Our results show that both the number and volume of ice-dammed lakes is expected to increase in the coming decades, regardless of climate change mitigation measures. As glaciers retreat, the area over which ice-dammed lakes can form will reduce after mid-century, eventually also reducing the number, size and volume of ice-dammed lakes. Whilst our results provide a regional perspective, further assessments are needed on a glacier-by-glacier basis to account for local factors that control lake formation and catastrophic drainage. Our results are nonetheless instrumental for the early identification of future hazards, as they provide the means of anticipating potentially large, future ice-dammed lakes. We argue that systematically accounting for ice-dammed lakes in future assessments of GLOF-related hazards is essential if damage to infrastructure and potential loss of life are to be prevented.

Methods

Model input data. To constrain glacier geometry, we use outlines of the Randolph Glacier Inventory version 6.0 (RGI 6.0⁴³). For the glacier surface, we use the Shuttle Radar Topography Mission DEM from 2000⁵⁰. For the ice thickness, we use the consensus estimate by ref. ⁵¹. The resolution of the surface DEM and ice thickness are of 25, 50, 100 and 200 m depending on glacier size⁵¹. Spatially distributed debris-cover thickness maps and glacier-specific Østrem curves (i.e., a function that defines the relation between debris-cover thicknesses and melt rates) are taken from ref. ⁵². To force the mass balance model (see below) in the past (2000–2020), we use 2m-temperature and precipitation data of the European Centre for Medium-Range Weather Forecasts re-analysis (ERA-5⁵³). For the future (2021–2100), we use the median (in terms of HMA-wide ice loss between 2020 and 2100 according to ref. ²⁶) Global Circulation Model (GCM) for each of the five SSP of the coupled model inter-comparison project phase 6 (CMIP6)²⁷. To merge the past and future series of air temperature and precipitation, the debiasing scheme of ref. ⁵⁴ is applied. The mass balance model is calibrated with geodetic mass balances available for every single glacier between 2000 and 2019³¹, and is validated against observations provided by the World Glacier Monitoring Service⁵⁵ (see ref. ²⁶ for details). Remote and in-situ observations of supraglacial debris-cover evolution of the last five decades are used to calibrate and validate the debris-cover evolution model²⁶.

Validation data. To validate the identification of ice-dammed lakes and their modelled evolution, we use the 30 m resolution dataset of ice-dammed lakes of ref. ²⁹, which covers all of HMA from 2008 to 2017 and contains a total of 1042 supraglacial lakes for the observational period. In addition, we use the 30 m resolution dataset of ref. ², which covers five additional glaciers (Ngozumpa O, Ngozumpa W, Rongbu, Lalaga, and Tsojo Glacier) between 1987 and 2020. The latter dataset contains 1534 supraglacial lakes in total. Note that the higher number of lakes in this second dataset is related to a higher accuracy in mapping also small lakes.

Glacier evolution. The Global Glacier Evolution Model "GloGEMflow"^{25,54} is used to calculate accumulation (solid precipitation and refreezing), ablation (with a degree day model), and ice flow (through the shallow ice approximation). The model also accounts for debris cover effects that enhance (thick debris layer) or reduce (thin debris layer) ice melt. Both the spatial distribution of supraglacial debris and the debris thickness evolve through time, which is achieved by using a parameterisation based on glacier mass balance and pre-existing debris coverage²⁶. Combining the surface DEM with the modelled rate of ice thickness change, we model the glacier evolution in three dimensions, thereby also including surface depressions.

Lake detection and evolution. Each year, we detect depressions on and adjacent to the evolving glacier surfaces, we assume these to be potentially water-filled, and use this procedure to identify the locations of potential ice-dammed lakes. Moraine-dammed lakes or proglacial lakes are excluded by omitting those lakes that do not drain through ice. This is done by filling bedrock depressions prior to the lake detection procedure. Once a potential ice-dammed lake is detected, its three-dimensional geometric evolution is modelled by accounting for the enhanced melt caused by the lake's presence^{4,28}. More specifically, the depth h (m) of the ice-dammed lake evolves through time t (years) as [Eq. 1]:

$$\frac{dh}{dt} = \begin{cases} (b_{z,t}^{\text{clean}} - b_{z,t}^{\text{debris}}) \cdot F \cdot \sqrt{\frac{1}{h}} & \text{if debris-covered glacier} \\ 0.2 \cdot b_{z,t}^{\text{clean}} \cdot F \cdot \sqrt{\frac{1}{h}} & \text{if clean-ice glacier} \end{cases} \quad (1)$$

where F is an energy-storage release factor ($\text{m}^{1/2}$, see below for details), $b_{z,t}^{\text{clean}}$ and $b_{z,t}^{\text{debris}}$ are the mass balances (m a^{-1}) at elevation z for clean and debris-covered ice, respectively (see ref. 26 for details), and the last term (i.e., $\sqrt{1/h}$) mimics water stratification^{48,56} by decreasing the lake's melt-in for deeper lakes (this is because surface water is often warmer than bottom water). Observations suggest that the energy absorbed by turbid water bodies—such as lakes commonly found on and in contact with debris-covered glaciers—cause melt rates that are comparable to clean-ice melt^{57–59}. Low-turbidity water bodies have a greater optical penetration depth, reducing albedo⁶⁰ and enhancing melt relative to an ice surface (e.g., ref. 61). The difference in albedo between supraglacial lakes and clean ice is typically between 0.2 and 0.3^{61,62}. In other studies modelling ice-dammed lakes in contact with clean ice glaciers (e.g., ref. 63), the additional melt underneath the water level was set to be equal to $b_{z,t}^{\text{clean}}$. Given the lack of data, we prefer to be conservative, and use 0.2 (-) as a multiplication factor for $b_{z,t}^{\text{clean}}$. A sensitivity analysis for this rather crude assumption is provided in the section “Sensitivity analysis” below. The factor F accounts for (1) the daily and seasonal sinusoidal behaviour of air temperature, which causes a part of the energy accumulated by the water during the day (summer) to be released to the atmosphere as long-wave radiation over night (late summer)^{45,47,48}, and (2) the background drainage of lake water, which evacuates accumulated energy. Based on the observations of ref. 48, we use $F = 0.8$. For analysing the uncertainties in F , a sensitivity study was performed (see again “Sensitivity analysis”).

We modify glacier lake geometry horizontally by prescribing a shoreline angle α (similarly to ref. 64). Ref. 49 measured shoreline angles of supraglacial lakes between 20° and 30°. Therefore, the horizontal evolution of each ice-dammed lake is modelled to maintain $\alpha \leq 20^\circ$ (again, see below for sensitivity analysis), while lakes can become deeper through Eq. (1). For this, the horizontal rate of shoreline growth perpendicular to the shoreline ($\frac{dl}{dt}$, in units of m a^{-1}) evolves through time as [Eq. 2]:

$$\frac{dl}{dt} = \frac{1}{\tan(\alpha)} \cdot h^{\text{lake}}, \quad (2)$$

where α is determined for the first 25 m from the shore (an arbitrary distance), and h^{lake} is the lake depth at 25 m distance from the shore.

We assess the plausibility of the so-obtained lake geometries by comparing the relationship between lake area and lake volume against the observations of ref. 65. We note a good agreement between these relationships for the present (Fig. 2c) and a slight temporal evolution of the volume-area relationship for the future. We attribute the latter to effects related to the spatial resolution of our model (see Supplementary Results, and Fig. S11).

Sensitivity analysis. Uncertainties in the evolution of ice-dammed lakes can arise from variations in the vertical and horizontal lake evolution. To test the sensitivity of our results, we re-computed the evolution of all ice-dammed lakes with $F = 1.0$ and $\alpha = 10^\circ$, as well as with $F = 0.6$ and $\alpha = 30^\circ$ (see Eq. (1)). The first and second set of parameters results in a faster and slower lake growth, respectively. Compared to the reference ($F = 0.8$ and $\alpha = 20^\circ$), the resulting total lake volume is between 58% larger and 27% smaller, respectively (shaded bands in Fig. 3d–f).

To model the future evolution of ice-dammed lakes, we use the median GCM for each of the five considered SSPs (here, “median” refers to the HMA-wide ice loss during 2020–2100 as determined by ref. 26). To analyse the model sensitivity to different GCMs of the same SSP, we re-compute the future evolution of all ice-dammed lakes with two other GCMs that differ by ± 1 standard deviations from the median (again in terms of HMA-wide ice loss). By the end of the century, this resulted in a deviation below $\pm 1\%$ in number, $\pm 3\%$ in area, and $\pm 2\%$ in volume of ice-dammed lakes compared to the median GCM (percentages refer to the mean difference over the period 2020–2100, see Fig. S12). This indicates that the computed lake evolution has low sensitivity with respect to the chosen GCM, especially when compared to the sensitivity associated to the lake evolution factors F and α (see above).

The depth h of the ice-dammed lake on clean-ice glaciers evolves through Eq. (1). To analyse the model sensitivity to the multiplication factor used to scale $b_{z,t}^{\text{clean}}$, we re-compute the future evolution of all ice-dammed lakes with multiplication factors of 0.1 and 0.3 (instead of the default value of 0.2). By the end of the century, this results in a deviation lower than $\pm 12\%$ in number, $\pm 10\%$ in area, and $\pm 24\%$ in

volume of lakes compared to the reference (Fig. S13). Although these variations are important, they show that the overall model sensitivity is dominated by the contributions of the lake evolution factors F and α .

Data availability

Output data of the model are accessible on <https://doi.org/10.3929/ethz-b-00055155466>.

Code availability

Code is available upon request.

Received: 13 April 2022; Accepted: 3 August 2022;

Published online: 26 August 2022

References

- Wang, X., Siegert, F., Zhou, A.-g & Franke, J. Glacier and glacial lake changes and their relationship in the context of climate change, Central Tibetan Plateau 1972–2010. *Global Planetary Change* **111**, 246–257 (2013).
- Nie, Y. et al. A regional-scale assessment of Himalayan glacial lake changes using satellite observations from 1990 to 2015. *Remote Sensing Environ.* **189**, 1–13 (2017).
- Shugar, D. H. et al. Rapid worldwide growth of glacial lakes since 1990. *Nat. Clim. Change* **10**, 939–945 (2020).
- King, O., Bhattacharya, A., Bhambri, R. & Bolch, T. Glacial lakes exacerbate Himalayan glacier mass loss. *Sci. Rep.* **9**, 1–9 (2019).
- Benn, D. et al. Response of debris-covered glaciers in the Mount Everest region to recent warming, and implications for outburst flood hazards. *Earth-Science Rev.* **114**, 156–174 (2012).
- Veh, G., Korup, O., von Specht, S., Roessner, S. & Walz, A. Unchanged frequency of moraine-dammed glacial lake outburst floods in the Himalaya. *Nat. Clim. Change* **9**, 379–383 (2019).
- Veh, G., Korup, O. & Walz, A. Hazard from Himalayan glacier lake outburst floods. *Proc. Natl Acad. Sci.* **117**, 907–912 (2020).
- Zheng, G. et al. Increasing risk of glacial lake outburst floods from future third pole deglaciation. *Nat. Clim. Change* **11**, 411–417 (2021).
- Stuart-Smith, R., Roe, G., Li, S. & Allen, M. Increased outburst flood hazard from lake Palcacocha due to human-induced glacier retreat. *Nat. Geosci.* **14**, 85–90 (2021).
- Iturrizaga, L. Lateroglacial valleys and landforms in the Karakoram Mountains (Pakistan). *GeoJournal* **54**, 397–428 (2001).
- Hewitt, K. *Glaciers of the Karakoram Himalaya* (Springer, 2014).
- Bazai, N. A. et al. Glacier surging controls glacier lake formation and outburst floods: the example of the Khurdopin Glacier, Karakoram. *Glob. Planetary Change* **208**, 103710 (2022).
- Veh, G. et al. Trends, breaks, and biases in the frequency of reported glacier lake outburst floods. *Earth's Future* **10**, e2021EF002426 (2022).
- Sattar, A. et al. Future glacial lake outburst flood (GLOF) hazard of the South Lhonak Lake, Sikkim Himalaya. *Geomorphology* **388**, 107783 (2021).
- Begam, S., Sen, D. & Dey, S. Moraine dam breach and glacial lake outburst flood generation by physical and numerical models. *J. Hydrol.* **563**, 694–710 (2018).
- Lala, J. M., Rounce, D. R. & McKinney, D. C. Modeling the glacial lake outburst flood process chain in the nepal himalaya: reassessing imja tsho's hazard. *Hydrol. Earth Syst. Sci.* **22**, 3721–3737 (2018).
- Zhang, T., Wang, W., Gao, T. & An, B. Simulation and assessment of future glacial lake outburst floods in the Poiqu river basin, Central Himalayas. *Water* **13**, 1376 (2021).
- Furian, W., Maussion, F. & Schneider, C. Projected 21st-century glacial lake evolution in High Mountain Asia. *Front. Earth Sci.* (2022).
- Vilímek, V., Emmer, A., Huggel, C., Schaub, Y. & Würmlí, S. Database of glacial lake outburst floods (GLOFs)—IPL project no. 179. *Landslides* **11**, 161–165 (2014).
- Harrison, S. et al. Climate change and the global pattern of moraine-dammed glacial lake outburst floods. *TCryosphere* **12**, 1195–1209 (2018).
- Racoviteanu, A. et al. Debris-covered glacier systems and associated glacial lake outburst flood hazards: challenges and prospects. *J. Geol. Soc.* **179** (2022).
- Nye, J. F. Water flow in glaciers: Jökulhlaups, tunnels and veins. *J. Glaciol.* **17**, 181–207 (1976).
- Bazai, N. A. et al. Increasing glacial lake outburst flood hazard in response to surge glaciers in the Karakoram. *Earth-Science Rev.* **212**, 103432 (2021).

24. GAPHAZ. *Assessment of Glacier and Permafrost Hazards in Mountain Regions – Technical Guidance Document*. Prepared by Allen, S. et al. pp. 72 (Standing Group on Glacier and Permafrost Hazards in Mountains (GAPHAZ) of the International Association of Cryospheric Sciences (IACS) and the International Permafrost Association (IPA). Zurich, Switzerland/Lima, Peru, 2017).
25. Zekollari, H., Huss, M. & Farinotti, D. Modelling the future evolution of glaciers in the European Alps under the EURO-CORDEX RCM ensemble. *Cryosphere* **13**, 1125–1146 (2019).
26. Compagno, L. et al. Modelling supraglacial debris-cover evolution from the single glacier to the regional scale: An application to High Mountain Asia. *Cryosphere Discuss.* **2021**, 1–33 (2021).
27. Eyring, V. et al. Overview of the Coupled Model Intercomparison Project Phase 6 (CMIP6) experimental design and organization. *Geosci. Model Dev.* **9**, 1937–1958 (2016).
28. Pronk, J. B. et al. Contrasting surface velocities between lake-and land-terminating glaciers in the Himalayan region. *Cryosphere* **15**, 5577–5599 (2021).
29. Chen, F. et al. Annual 30 m dataset for glacial lakes in high mountain asia from 2008 to 2017. *Earth Syst. Sci. Data* **13**, 741–766 (2021).
30. Farinotti, D., Immerzeel, W. W., de Kok, R. J., Quincey, D. J. & Dehecq, A. Manifestations and mechanisms of the Karakoram glacier anomaly. *Nat. Geosci.* **13**, 8–16 (2020).
31. Hugonnet, R. et al. Accelerated global glacier mass loss in the early twenty-first century. *Nature* **592**, 726–731 (2021).
32. Brun, F., Berthier, E., Wagnon, P., Käab, A. & Treichler, D. A spatially resolved estimate of High Mountain Asia glacier mass balances from 2000 to 2016. *Nat. Geosci.* **10**, 668–673 (2017).
33. Rounce, D. R., Hock, R. & Shean, D. Glacier mass change in High Mountain Asia through 2100 using the open-source Python Glacier Evolution Model (PyGEM). *Front. Earth Sci.* **7**, 331 (2020).
34. Kraaijenbrink, P. D. A., Bierkens, M. F. P., Lutz, A. F. & Immerzeel, W. W. Impact of a global temperature rise of 1.5 degrees Celsius on Asia's glaciers. *Nature* **549**, 257–260 (2017).
35. Marzeion, B. et al. Partitioning the uncertainty of ensemble projections of global glacier mass change. *Earth's Future* **8**, e2019EF001470 (2020).
36. Maurer, J. M., Schaefer, J., Rupper, S. & Corley, A. Acceleration of ice loss across the Himalayas over the past 40 years. *Sci. Adv.* **5**, eaav7266 (2019).
37. Shean, D. E. et al. A systematic, regional assessment of High Mountain Asia glacier mass balance. *Front. Earth Sci.* **7**, 363 (2020).
38. Clague, J. & Mathews, W. The magnitude of jökulhlaups. *J. Glaciol.* **12**, 501–504 (1973).
39. Haemmig, C. et al. Hazard assessment of glacial lake outburst floods from Kyagar glacier, Karakoram mountains, China. *Ann. Glaciol.* **55**, 34–44 (2014).
40. Round, V., Leinss, S., Huss, M., Haemmig, C. & Hajnsek, I. Surge dynamics and lake outbursts of Kyagar Glacier, Karakoram. *Cryosphere* **11**, 723–739 (2017).
41. Meier, M. F. & Post, A. What are glacier surges? *Canad. J. Earth Sci.* **6**, 807–817 (1969).
42. Benn, D., Fowler, A. C., Hewitt, I. & Sevestre, H. A general theory of glacier surges. *J. Glaciol.* **65**, 701–716 (2019).
43. RGI Consortium. Randolph Glacier Inventory 6.0 (2017).
44. Benedek, C. L. & Willis, I. C. Winter drainage of surface lakes on the Greenland Ice Sheet from Sentinel-1 SAR imagery. *Cryosphere* **15**, 1587–1606 (2021).
45. Chikita, K., Jha, J. & Yamada, T. Hydrodynamics of a supraglacial lake and its effect on the basin expansion: Tsho Rolpa, Rolwaling Valley, Nepal Himalaya. *Arctic Antarctic Alpine Res.* **31**, 58–70 (1999).
46. Tweed, F. S. & Russell, A. J. Controls on the formation and sudden drainage of glacier-impounded lakes: Implications for jökulhlaup characteristics. *Prog. Phys. Geogr.* **23**, 79–110 (1999).
47. Sakai, A., Takeuchi, N., Fujita, K. & Nakawo, M. Role of supraglacial ponds in the ablation process of a debris-covered glacier in the nepal himalayas. *Int. Assoc. Hydrol. Sci.* **264**, 119–130 (2000).
48. Wang, X. et al. Thermal regime of a supraglacial lake on the debris-covered Koxkar Glacier, southwest Tianshan, China. *Environ. Earth Sci.* **67**, 175–183 (2012).
49. Mertes, J. R., Thompson, S. S., Booth, A. D., Gullep, J. D. & Benn, D. I. A conceptual model of supra-glacial lake formation on debris-covered glaciers based on GPR facies analysis. *Earth Surf. Proc. Landforms* **42**, 903–914 (2017).
50. Farr, T. G. et al. The shuttle radar topography mission. *Rev. Geophys.* **45**, RG2004 (2007).
51. Farinotti, D. et al. A consensus estimate for the ice thickness distribution of all glaciers on earth. *Nat. Geosci.* **12**, 168–173 (2019).
52. McCarthy, M. et al. Supraglacial debris thickness and supply rate in High Mountain Asia. *Commun. Earth Environ.* (2021, preprint).
53. Hersbach, H. et al. Global reanalysis: goodbye ERA-Interim, hello ERA5. *ECMWF* **3**, e2011834–e2011834 (2019).
54. Huss, M. & Hock, R. A new model for global glacier change and sea-level rise. *Front. Earth Sci.* **3**, 54 (2015).
55. WGMS. Fluctuations of glaciers database (2020).
56. Röhl, K. Thermo-erosional notch development at fresh-water-calving Tasman Glacier, New Zealand. *J. Glaciol.* **52**, 203–213 (2006).
57. Miles, E. S. et al. Surface pond energy absorption across four Himalayan glaciers accounts for 1/8 of total catchment ice loss. *Geophys. Res. Lett.* **45**, 10–464 (2018).
58. Rounce, D. R. et al. Distributed global debris thickness estimates reveal debris significantly impacts glacier mass balance. *Geophys. Res. Lett.* **48**, e2020GL091311 (2021).
59. Miles, E., Steiner, J., Buri, P., Immerzeel, W. & Pellicciotti, F. Controls on the relative melt rates of debris-covered glacier surfaces. *Environ. Res. Lett.* **17**, 064004 (2022).
60. Tedesco, M. & Steiner, N. In-situ multispectral and bathymetric measurements over a supraglacial lake in western Greenland using a remotely controlled watercraft. *Cryosphere* **5**, 445–452 (2011).
61. Lüthje, M., Pedersen, L. T., Reeh, N. & Greuell, W. Modelling the evolution of supraglacial lakes on the west Greenland ice-sheet margin. *J. Glaciol.* **52**, 608–618 (2006).
62. Benn, D., Wiseman, S. & Hands, K. Growth and drainage of supraglacial lakes on debris-mantled Ngozumpa Glacier, Khumbu Himal, Nepal. *J. Glaciol.* **47**, 626–638 (2001).
63. Huss, M., Voinesco, A. & Hoelzle, M. Implications of climate change on glacier de la Plaine Morte, Switzerland. *Geographica Helvetica* **68**, 227–237 (2013).
64. Käab, A. & Haeblerli, W. Evolution of a high-mountain thermokarst lake in the Swiss Alps. *Arctic Antarctic Alpine Res.* **33**, 385–390 (2001).
65. Cook, S. & Quincey, D. Estimating the volume of Alpine glacial lakes. *Earth Surf. Dynam.* **3**, 559–575 (2015).
66. Compagno, L., Huss, M., Zekollari, H., Miles, E. S. & Farinotti, D. Future growth and decline of high mountain asia's ice-dammed lakes and associated risk (dataset). *ETH Zurich Res. Collect.* (2022).
67. Nie, Y. et al. Glacial change and hydrological implications in the Himalaya and Karakoram. *Nat. Rev. Earth Environ.* **2**, 91–106 (2021).
68. Guillet, G. et al. A regionally resolved inventory of high mountain asia surge-type glaciers, derived from a multi-factor remote sensing approach. *Cryosphere* **16**, 603–623 (2022).

Acknowledgements

We thank Georg Veh, who provided the Glacial Lake Outburst Flood Database and important related information. We are grateful to the Swiss National Science Foundation, and for the funding of project Nr. 184634 in particular. Harry Zekollari acknowledges the funding from the Fonds de la Recherche Scientifique (FNRS postdoctoral fellowship). This publication was supported by PROTECT and RAVEN. This project has received funding from the European Union's Horizon 2020 research and innovation programme under grant agreements Nos. 869304 (PROTECT) and 772751 (RAVEN), PROTECT contribution number 38. We thank the RGI consortium for the global glacier inventory data. We acknowledge the ECMWF for the ERA-5 re-analysis, and CMIP for the GCM outputs. We also thank the WGMS for providing mass balance and length change measurements.

Author contributions

L.C., M.H., H.Z., E.S.M. and D.F. conceived the study. L.C. wrote the lake detection and evolution code, and performed the numerical modelling with support from M.H., H.Z., E.S.M. and D.F. The GloGEMflow code was developed by M.H. (mass balance and debris evolution modules) and by H.Z. (ice flow module). L.C. wrote the paper and produced the figures, with contributions from all other co-authors.

Competing interests

The authors declare no competing interests.

Additional information

Supplementary information The online version contains supplementary material available at <https://doi.org/10.1038/s43247-022-00520-8>.

Correspondence and requests for materials should be addressed to Loris Compagno.

Peer review information *Communications Earth Environment* thanks the anonymous reviewers for their contribution to the peer review of this work. Primary Handling Editors: Joe Aslin, Heike Langenberg.

Reprints and permission information is available at <http://www.nature.com/reprints>

Publisher's note Springer Nature remains neutral with regard to jurisdictional claims in published maps and institutional affiliations.



Open Access This article is licensed under a Creative Commons Attribution 4.0 International License, which permits use, sharing, adaptation, distribution and reproduction in any medium or format, as long as you give appropriate credit to the original author(s) and the source, provide a link to the Creative Commons license, and indicate if changes were made. The images or other third party material in this article are included in the article's Creative Commons license, unless indicated otherwise in a credit line to the material. If material is not included in the article's Creative Commons license and your intended use is not permitted by statutory regulation or exceeds the permitted use, you will need to obtain permission directly from the copyright holder. To view a copy of this license, visit <http://creativecommons.org/licenses/by/4.0/>.

© The Author(s) 2022